

PAPER

Alpha half-lives calculation of superheavy nuclei with Q_α -value predictions based on the Bayesian neural network approach


To cite this article: Ubaldo Baños Rodríguez *et al* 2019 *J. Phys. G: Nucl. Part. Phys.* **46** 115109

View the [article online](#) for updates and enhancements.

You may also like

- [Shell closures in FI superheavy isotopes via determination of alpha decay preformation factor](#)
Norah A M Alsaif, Shahidan Radiman and Saad M Saleh Ahmed
- [Microscopic description of the alpha-decay of a superheavy element](#)
A. Sandulescu, M. Mirea and D. S. Delion
- [Alpha and heavy cluster radioactivity of superheavy nuclei 100 \$Z\$ 120](#)
GM Carmel Vigila Bai and R Revathi

Alpha half-lives calculation of superheavy nuclei with Q_α -value predictions based on the Bayesian neural network approach

Ubaldo Baños Rodríguez^{1,5}, Cristofher Zuñiga Vargas^{1,2},
Marcello Gonçalves³, Sergio Barbosa Duarte¹  and
Fernando Guzmán⁴

¹Centro Brasileiro de Pesquisas Físicas (CBPF), Rua Dr. Xavier Sigaud 150, 22290-180 Rio de Janeiro-RJ, Brazil

²Departamento de Física, Universidade Federal do Maranhão (UFMA), Campus Universitário do Bacanga, 65085-580, São Luís, Maranhão, Brazil

³Comissão Nacional de Energia Nuclear, R. Gal. Severiano, 22290-151, Rio de Janeiro, Brazil

⁴Instituto Superior de Tecnologías y Ciencias Aplicadas(InSTEC), Havana University. Ave. Salvador Allende y Luaces Havana 10400, AP 6163, La Habana, Cuba

E-mail: ubaldo@cbpf.br

Received 5 April 2019, revised 6 June 2019

Accepted for publication 25 June 2019

Published 3 October 2019



CrossMark

Abstract

In this work, we performed a systematic study of the α -decay process by employing the Bayesian neural network approach. The Q_α -value prediction of the ten parameter Duflo-Zuker mass model has been improved from a root-mean-square deviation relative to the experimental data $\sigma = 0.43$ MeV to $\sigma = 0.122$ MeV. This correction brought to light some missing physical aspects in the DZ mass model, so as to identify some magic numbers not present in the original model. By using a phenomenological effective model to deal with alpha decay half-lives, we were able to obtain the half-life values throughout the superheavy elements region. As a main result, we found that the region of greatest stability against the alpha-decay process for superheavy elements is between $106 \leq Z \leq 110$ and $180 \leq N \leq 184$.

Keywords: alpha decay, Bayesian neural network, superheavy elements

(Some figures may appear in colour only in the online journal)

⁵ Author to whom correspondence should be addressed.

1. Introduction

The α -decay of transactinide elements, also referred to as superheavy elements (SHE)–nuclides with an atomic number above the Rutherfordium element–has arisen great interest since it constitutes, in competition with the spontaneous fission (SF), the main decay mechanisms of these nuclei. At the same time, the α -decay process is one of the main sources of knowledge of the nuclear level structure, by allowing us to experimentally confirm the predictions of proposed theoretical models. In the last 20 years, the number of works published with interest in the SHE region has been gradually increased (see a comprehensive review of [1] and references therein, as well as [2]). To date, the heaviest element known is named oganesson with the chemical symbol Og, and atomic number $Z = 118$ [3].

Since the early works of Gamow [4], Condon and Gurney [5] to the present, many phenomenological and microscopic models have been proposed. The effective liquid drop model (ELDM) has been successfully applied to determine α -decay half-lives [6–15]. In the present approach, the cluster-like mode is used considering that the alpha particle is pre-formed inside the parent nucleus and emitted after tunneling an effective potential barrier. In the last few years, many experimental α -decay half-life and energy released have been measured [3, 16–18]. These half-life values have been well reproduced with the ELDM. A crucial element in the α -decay half-life calculation is the energy released in the process, the Q_α -value. When the Q_α -value is not available experimentally it can be determined from the mass difference of the involved nuclei,

$$Q_\alpha \equiv [M_p - (M_d + M_\alpha)], \quad (1)$$

where M_p , M_d , M_α represent the nuclear mass of the parent, daughter nucleus and alpha-emitted particle, respectively. As most of the SHE mass is still unknown, we employed in our calculation the newest experimental mass values from [19].

Due to the limitation of mass models in predicting some physical phenomena, as well as to the associated uncertainties of the experimental data, there are still significant deviations between the experimental and the predicted values. In the last few years, many works have appeared using machine learning methods to perform descriptions or predictions based on the available data [20–26]. In this work, we aim to improve the predictive power of nuclear mass models in respect to the alpha released energy calculation, by using the machine learning methodology. Following the methodology developed in these works [25, 27–35] based on the Bayesian neural network (BNN) [36, 37], we constructed a residual correction to the modelled Q_α energy directly using experimental available values. Thus we can extend the α -decay released energies calculation to regions where experimental data is not available. Olsen and Nazarewicz in [38] suggested independently (still as a proposal) the use of Bayesian methods to improve the prediction of Q_α values. The main goal of this work is the study of the SHE region through the released energy and half-life values for the alpha decay process, investigating the nucleus stability against the α -decay mechanism and determining magic numbers not predicted by the model.

This work is presented as follows. In section 2 we describe briefly the BNN methodology to improve the Q -value used in the ELDM. In section 3 the α -decay model main ideas are reviewed; section 6 is devoted to reporting and discussing our results. Finally, section 7 summarizes our conclusions.

2. Bayesian neural network approach

A detailed description of the Bayesian neural network method can be found in [36]. Here we only highlight the main features of the approach. The parameters of the network, θ , are calculated from the Bayes theorem, being necessary to introduce a probability distribution function $\pi(\theta)$ of these parameters, so-called prior distribution. Therefore, the Bayes theorem asserts that the posterior distribution, $\mathcal{P}(\theta|\mathcal{D})$, can be calculated as:

$$\mathcal{P}(\theta|\mathcal{D}) = \frac{\mathcal{L}(\mathcal{D}|\theta)\pi(\theta)}{\mathcal{E}(\mathcal{D})}, \quad (2)$$

where $\mathcal{L}(\mathcal{D}|\theta)$ is the likelihood function, $\pi(\theta)$ is the prior distribution of the parameters θ and $\mathcal{E}(\mathcal{D})$ is a normalization constant that represents the evidence of the model. The data sets are given by $\mathcal{D} = \{(x_1, t_1), (x_2, t_2), \dots, (x_N, t_N)\}$, where x_i and t_i denote the i -th relevant input and output data, respectively, and N is the number of available data.

In order to perform a Bayesian neural network analysis, we consider the multivariate Gaussian likelihood function, as being as follows

$$\mathcal{L}(\mathcal{D}|\theta) \propto \exp\left[-\frac{\chi^2(\mathcal{D}|\theta)}{2}\right], \quad (3)$$

where the objective function χ^2 reads

$$\chi^2(\mathcal{D}|\theta) = \sum_{i=1}^N \left[\frac{t_i - \psi(x_i, \theta)}{\delta t_i} \right]^2, \quad (4)$$

with $t_i \equiv t(x_i)$ being the empirical value of the target evaluated at the i -th input data x_i and its associated error given by δt_i . For the BNN approach the function $\psi(x_i, \theta)$, which expresses the relationship between the input and output data, is described in terms of a neural network as:

$$\psi(\mathbf{x}, \theta) = a + \sum_{j=1}^H b_j \tanh\left[c_j + \sum_{i=1}^I d_{ji}x_i\right], \quad (5)$$

where \mathbf{x} represents the input data, $\theta = \{a, b_j, c_j, d_{ji}\}$ are the model free parameters, H is the number of neurons in the hidden layer, I the number of input units. The prior distributions are assumed as being Gaussian functions with zero mean and variance values, modelled by a gamma distribution. Having defined the posterior parameters distribution $\mathcal{P}(\theta|\mathcal{D})$ as proportional to the product of the likelihood function $\mathcal{L}(\mathcal{D}|\theta)$ and the prior distribution $\pi(\theta)$, we are able to perform some predictions by averaging the neural network over the posterior probability density functions,

$$\langle \psi \rangle = \int \psi(\mathbf{x}, \theta) \mathcal{P}(\theta|\mathcal{D}) d\theta = \frac{1}{m} \sum_{j=1}^m \psi(x_j, \theta_j). \quad (6)$$

Due to the large dimensionality of the equation (6), Monte Carlo integration algorithms were used in its solution. To sample the posterior distribution, we used the Markov chain Monte Carlo method developed by Neal [36]. Since the model's parameters are described with a probability distribution function, the predictions of statistical uncertainty of these functions can be obtained as

$$\Delta\psi = \sqrt{\langle \psi^2 \rangle - \langle \psi \rangle^2}. \quad (7)$$

After the brief introduction above presented, the concept of energy released in a α -decay process is used in the BNN algorithm to reconstruct the residual energy released difference between the experimental and the model predicted values:

$$\delta_{\alpha}^{\text{BNN}}(\mathbf{x}) = Q_{\alpha}^{\text{Exp}}(Z, N) - Q_{\alpha}^{\text{Th}}(Z, N), \quad (8)$$

where the predicted α released energy $Q_{\alpha}^{\text{Th}}(Z, N)$ quantity is defined as follows:

$$Q_{\alpha}^{\text{Th}}(Z, N) = M^{\text{Th}}(Z, N) - M^{\text{Th}}(Z - 2, N - 2) - M_{\alpha}, \quad (9)$$

where $M^{\text{Th}}(Z, N)$ and $M^{\text{Th}}(Z - 2, N - 2)$ are obtained from the ten-parameters Duflo-Zuker (DZ) mass model [39], and the alpha particle mass M_{α} is taken from the data. Finally our corrected alpha released energy model is constructed as follows:

$$Q_{\alpha}^{\text{BNN}}(Z, N) \equiv Q_{\alpha}^{\text{Th}}(Z, N) + \delta_{\alpha}^{\text{BNN}}(\mathbf{x}). \quad (10)$$

3. Semiclassical approaches for alpha decay half-lives

The α -decay half-lives were calculated following the Gonçalves and Duarte [6, 11] potential model, using the so-called cluster-like framework. In this model the mass of the fragments does not vary during the molecular phase of the fragmentation process and the inertia coefficient of the system is determined by the Werner–Wheeler’s approximation for an incompressible and irrotational nuclear flow. A detailed description of the approach can be found in references [6–15]. Here we highlight the main features of the approach, describing expressions for Gamow’s alpha-decay factor for the final value of the decay rate for a spherical system with a barrier height $V(r) - Q_{\alpha}^{\text{BNN}}$.

By defining the decay constant as $\lambda = \nu_0 P_{\alpha}$, the alpha decay half-life can be obtained as:

$$\tau_{\alpha} = \frac{\ln(2)}{\nu_0 P_{\alpha}}, \quad (11)$$

where ν_0 is a free parameter associated with the alpha preformation probability. The value of this parameter together with the parameter r_0 used to determine the nuclear radius are established in order to obtain the best agreement with the half-life experimental data. The barrier penetrability factor P_{α} is given by:

$$P_{\alpha} = \exp^{-G_{\alpha}}, \quad (12)$$

where G_{α} is the Gamow’s factor related to tunneling through the barrier. This is given by the classical Wentzel–Kramers–Brillouin (WKB) approximation:

$$G_{\alpha} = -\frac{2}{\hbar} \int_{R_1}^{R_2} \sqrt{2\mu_{\text{WW}}^{\text{CMAS}}(r)[V_{\text{eff}}(r) - Q_{\alpha}^{\text{BNN}}]} dr. \quad (13)$$

Here r is the separation between the centers of the emitted α particle and the residual nucleus; $V_{\text{eff}}(r)$ is the effective potential; $\mu_{\text{WW}}^{\text{CMAS}}$ is the reduced mass of the system using the Werner–Wheeler’s approximation [6]; $Q_{\alpha}^{\text{BNN}}(\mathbf{x})$ is the Bayesian corrected alpha released energy for the α -decay process, see equation (10). The quantity R_1 and R_2 are classical turning points, defined by the condition $V(R_1) = V(R_2) = Q_{\alpha}^{\text{BNN}}(\mathbf{x})$. The effective potential is defined by the Coulomb, the surface and the angular potential contributions, i.e., $V(r) = V_c(r) + V_s(r) + V_{\ell}(r)$ (ℓ is the angular momentum of the system) [6, 11]. Where the surface tension energy coefficient is calculated (σ_{eff}) through the equation:

$$\frac{3}{5}e^2 \left[\frac{Z_p^2}{R_p} - \frac{Z_\alpha^2}{R_\alpha} - \frac{Z_D^2}{R_D} \right] + 4\pi\sigma_{\text{eff}}(R_p^2 + \bar{R}_\alpha^2 + \bar{R}_D^2) = Q_\alpha^{\text{BNN}}(\mathbf{x}), \quad (14)$$

and $Z_i e$ ($i = p, \alpha, D$) are the nuclear charge of the parent nucleus, the α -particle, and the daughter nucleus, respectively.

The final radii of the fragment should be given in terms of the parent radius by

$$\bar{R}_i = \left(\frac{Z_i}{Z_p} \right)^{1/3} R_p, \quad i = \alpha, D, \quad (15)$$

to be consistent with the uniform charge distribution considered in the Coulomb potential. The radius of the parent nuclei is determined by the expression $R_p = r_0 A^{1/3}$. The definition for the surface tension establishes the effective character of the model, since the difference between the energies of the initial and final configurations of the system reproduces the alpha-released energy $Q_\alpha^{\text{BNN}}(\mathbf{x})$.

At this point, we remark the importance of the $Q_\alpha^{\text{BNN}}(\mathbf{x})$ value to determine the half-life values. Firstly, due to its explicit presence in the Gamow penetrability factor equation (13) and then owing to the fact that it partially brings to the model many nuclear structural aspects like shell effects and nucleon pairing through the surface tension (14) ingredient.

4. Ten-parameter Duflo-Zuker mass model fitting

The mass model used to determine the main contribution of α -decay Q_α -values should be adjusted to the chosen set of experimental data extracted from AME2016 [19]. Our choice of mass model was the ten-parameter DZ model [39]. This mass model is chosen due to its simplicity and also because it presents a small standard deviation in respect to the experimental data. Hence, the first task is to obtain the set of parameters which better fit the data. Since the accuracy of the fitting can depend on the nuclear region where the model is applied, we decided to consider the nuclei available in the AME2016 database [19] with $Z > 52$. In addition we have taken into account only data with experimental uncertainty in the mass value, σ_{exp} , smaller than 100 keV. We regarded a total of 1355 nuclei in the fitting process of DZ mass model parameters. The values of the parameters that best fit the data are shown in table 1, with the deviation between the model results and experimental data, σ , presented in the last row column.

5. Bayesian neural networks: applied procedure for the α -decay process

To define our neural network to calculate the Q_α -values for a given nucleus, we employed a four-dimensional input vector composed by: (i) the atomic number, (ii) the number of neutrons, (iii) the difference between the atomic numbers and the closest magic number {8, 20, 28, 50, 82, 126}, (iv) and the difference between the number of neutrons and its closest magic number {8, 20, 28, 50, 82, 126, 184}. Therefore the four-component input vector is $\mathbf{x} = (Z, N, d_p, d_n)$, where $d_p = |Z - Z_k|$ and $d_n = |N - N_k|$ (Z_k and N_k being the closest magical number for protons and neutrons, respectively). With the four-dimension input vector and 17 hidden neurons ($H = 17$) our neural network has a total of 103 parameters.

Note that the experimental Q_α -value of each process is extracted directly from the AME2016 database [19]. A total of 443 alpha emitters were collected in the range $52 \leq Z \leq 118$, being 131 even-even (e-e), 95 odd-odd (o-o), 121 even-odd (e-o) and 96

Table 1. Values for the ten-parameter Duflo-Zuker model [39], by fitting 1355 experimental nuclear mass with $Z \geq 52$ and uncertainty smaller than 100 keV. The corresponding standard root-mean-square deviations (σ) from the experimental data are given at the end (in MeV).

σ	a_3	a_1	a_2	a_4	a_5	a_7	a_8	a_9	a_{10}	a_6	σ (MeV)
0.699		17.577	15.557	36.333	48.291	0.370	1.585	0.021	41.033	6.261	0.445

Table 2. Deviations of the alpha released energy calculated with the ten-parameter DZ mass model. Separated into two rows (training subset and testing subset). In the second column we present the σ value without BNN correction, in the third column the σ value with BNN correction, and in the forth column the relative difference between them.

	σ_{pre} (MeV)	σ_{post} (MeV)	$\Delta\sigma/\sigma_{\text{pre}}$
Training subset	0.444	0.178	0.60
Testing subset	0.403	0.247	0.38

odd–even (o–e) nuclei. With the structure of the neural network defined, as well as the experimental Q_α data set selected, we are able to validate the predictive power of our implemented BNN refinement procedure. Thus, the entire experimental Q_α data is separated into two different subsets: the training and testing subsets. To determine the value of the parameters of the neural network, see equation (5), we use the training subset. This procedure is called calibration of the neural network. Once our neural network is calibrated, we verify its predictive power by determining the values of the remaining experimental data which we have separated in the testing subset. Our training subset is formed by 364 randomly selected nuclei, and the remaining 79 nuclei composing the testing subset.

After several essays for calibration of the neural network for different training and test subsets, we obtained a continuous improvement of the Q_α -values in the context of the DZ mass model. A typical result for one of these essays is displayed in table 2.

The training subset improves by 60% from $\sigma_{\text{pre}} = 0.444$ to $\sigma_{\text{post}} = 0.178$. When the BNN correction was applied to the testing subset, the improvement was somewhat smaller (around 38%). This represents a change from $\sigma_{\text{pre}} = 0.403$ to $\sigma_{\text{post}} = 0.247$. This exhibits the predictive power of the BNN. Thus we calibrate the neural network with the whole set of 443 experimental data available, and predict the Q_α -values in regions of (Z, N) where experimental data is not yet available.

6. Results and discussion

When we calibrated the neural network with the 443 Q_α experimental data, the standard deviation improvement was 72%, i.e. it varied from $\sigma = 0.432$ MeV to $\sigma = 0.122$ MeV. The difference between experimental and calculated Q_α values with and without BNN correction, is shown in figure 1. The deviations between the mass model corrected with the BNN algorithm (Q_α^{BNN}) and experimental results clearly decrease, asserting the importance of the BNN correction. It should be noted that the largest deviations occur in the SHE region (the gray shadow in the figure 1). These results point to the importance of focusing attention in predictions in this region, where data is very scarce.

Besides the evident improvement in the Q_α -value prediction, it is possible to reveal some aspects of the SHE nuclei structure, mainly by identifying some magic or sub-magic numbers. Nuclei with magic or sub-magic numbers must be relatively more stable than their neighboring nuclei and a local minimum in Q_α curve vs neutron number of the parent nucleus, N , could be very elucidative. Hence, we presented in figures 2 and 3 the alpha-decay released energy as a function of the neutron number for nuclei between Rf ($Z=104$) and Og ($Z=118$), separated in four groups of SHE isotopes, covering the set of existing experimental data.

In figure 2 we show the alpha-decay released energy calculated with the DZ mass model. We can see that the DZ mass model roughly describes the behavior of data, despite,

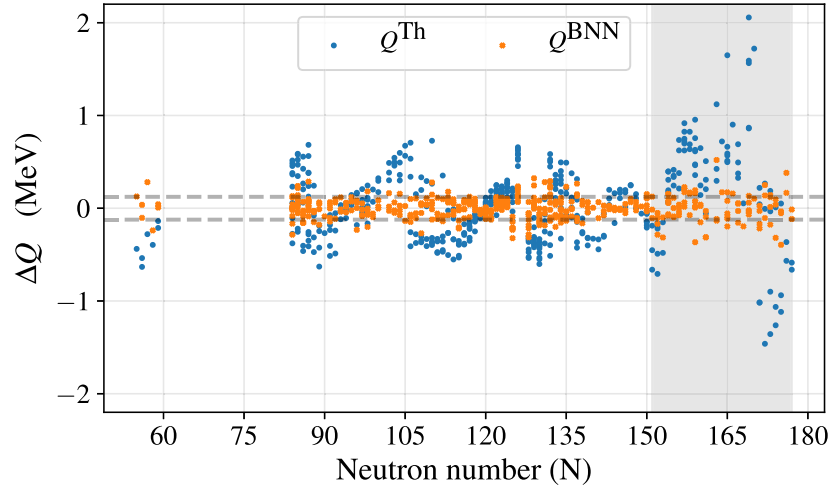


Figure 1. The difference between theoretical and experimental alpha energy released. Points labeled Q_{α}^{Th} and Q_{α}^{BNN} are the results of DZ and DZ + BNN calculation, respectively. The gray shade defines the SHE region where the corrections are most significant.

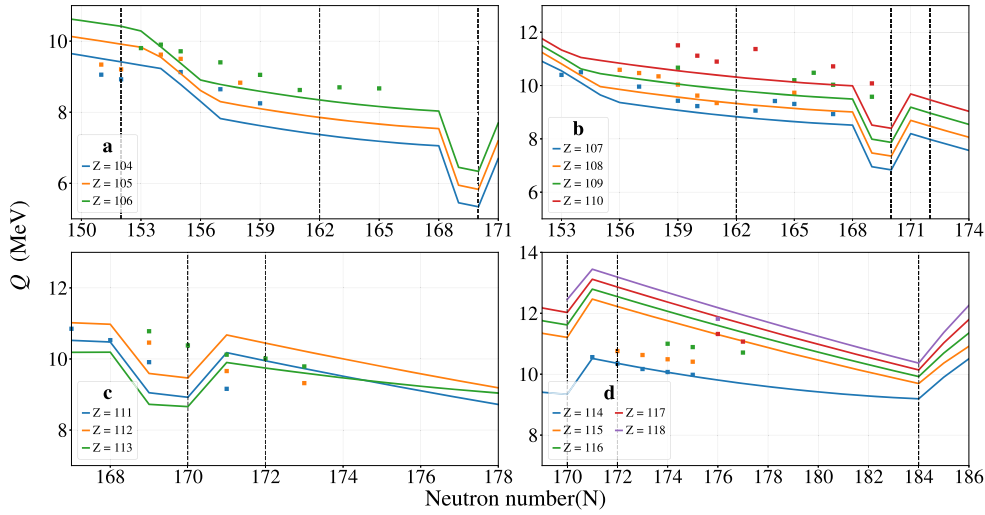


Figure 2. Released energy of the alpha-decay process, Q_{α} , obtained with the DZ mass model as a function of neutron numbers N , in the selected SHE region $104 \leq Z \leq 118$. Line and dots represent the calculated and experimental value, respectively. The dashed vertical black lines represent some possible magic or sub-magic numbers extracted from [16] and references cited therein.

quantitatively, the deviation still being significant between theoretical and experimental values. For this region, the standard deviation is $\sigma = 0.73$ MeV. Another important element to notice is the decrease of the Q_{α} -value in the region $168 \leq N \leq 171$ for all SHE's, and at $N = 184$ for elements between Cn ($Z = 112$) and Og ($Z = 118$). The latter is only shown in panel (d) for the nuclei represented there. According to the DZ model prediction, the two

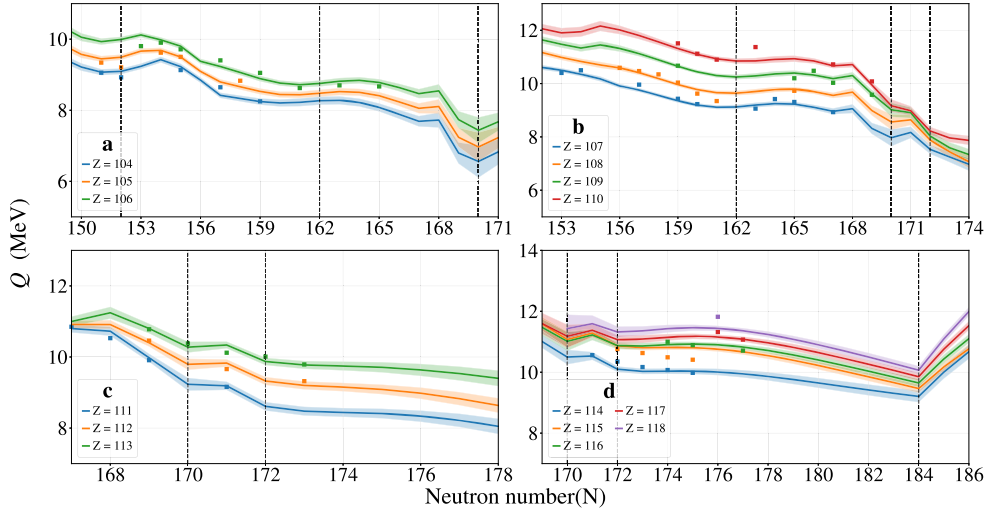


Figure 3. The same as figure 2 but Q_α -values obtained with the DZ + BNN correction. The shaded area represents the Q_α^{BNN} uncertainty.

regions mentioned above have an increase in stability, which may reflect on the closure of a neutron shell or sub-shell.

In figure 3 results for the BNN correction of the alpha-decay released energy is displayed. In this figure, the shaded area represents the Q_α^{BNN} one-sigma uncertainty, associated with the BNN approach calculation. As we can see, most of the data is quite well reproduced by the improved predictions or remains within one-sigma uncertainty level. Results presenting the larger deviation between theoretical and experimental values, ΔQ_α , have been obtained for ^{259}Sg , ^{269}Hs , ^{273}Ds , ^{272}Rg , ^{289}Mc , ^{290}Mc and ^{294}Og nuclei, where $|\Delta Q_\alpha| = 0.32, 0.31, 0.52, 0.31, 0.32, 0.39$ and 0.38 MeV, respectively. Despite these differences, in this region the BNN approach provided a decrease in the rms to $\sigma = 0.16$ MeV, meaning an improvement of 78% compared to the previous $\sigma = 0.73$ MeV. Note that in figure 3 the qualitative behavior of the curves changes and the BNN corrected curve seems to be more precise at the magic or sub-magic neutron numbers.

Also, observe in region (a) of figure 3, there are three local minima, two of them are very close to previously neutron magic numbers reported in other works (see [16] and references therein). Here, these minima are highlighted by the BNN procedure, being located near $N \sim 152$ and 162 . On the other hand, the minimum located in the region $168 \leq N \leq 171$ was also predicted by the model and persists for all the regions of figure 3. In region (b) a new shallow local minimum appears at $N \sim 162$, which is reported in previous work (see [16] and references therein) as the number of neutrons in the island of deformed nuclei centered at ^{270}Hs . In regions (b), (c) and (d) the depth of the local minimum in $168 \leq N \leq 171$ is markedly softened in respect to the corresponding region on figure 2. Thus, the employment of the BNN model clearly turns theoretical Q_α -values closer to the data. This improvement results in a softening of the curves mainly as the parent atomic number increases. The expected magic number $N = 172$ is rather not evident in the figure and further experimental investigation may be needed to confirm this value. However, the magic number candidate predicted by the DZ mass model at $N \sim 184$ undoubtedly persisted with the BNN correction,

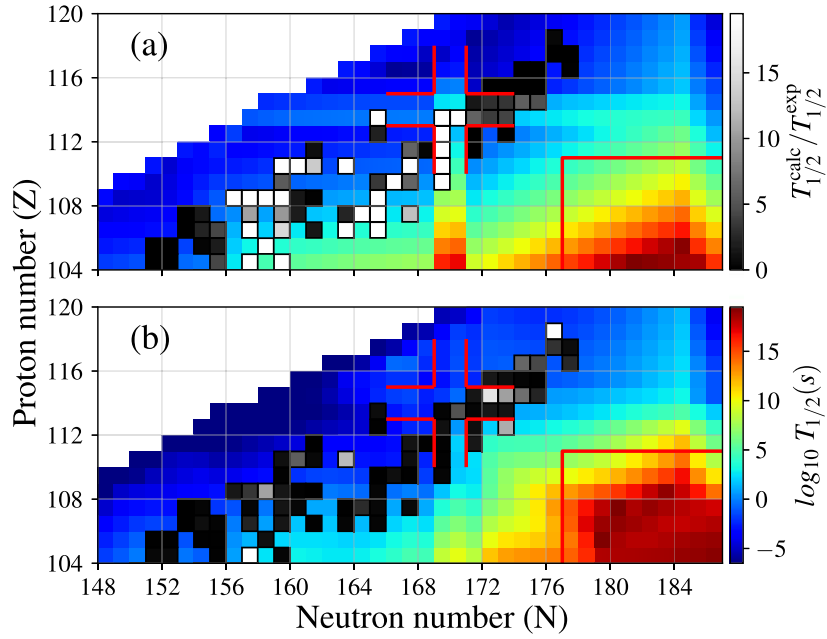


Figure 4. Nuclear chart for the SHE region, showing the alpha-decay half-life values. Experimental half-life is marked with black frames. The ratio between the theoretical and the experimental values is displayed in grayscale. In part (a) results were obtained with the DZ mass model and in (b) results were obtained with the DZ + BNN correction.

asserting that other elements heavier than Og may be found in future experiments also posing the $N = 184$ magic shell.

The main goal of this work is to make predictions of α -decay half-lives for SHE considering the ELDM [6, 11] and taking into account, the Q_{α}^{BNN} -values obtained with the BNN correction. In the context of the ELDM, the alpha preformation factor ν_0 and the radius coefficient $r_0 = R_0/A^{1/3}$ must be taken as parameters. The choice of values for these quantities was performed to reproduce experimental data. Thus, by determining the minimum for the root-mean-square value of the expression

$$\sigma = \sqrt{\frac{1}{w-1} \sum_{i=1}^w [\log_{10}(\tau_{\text{Exp}}^i / \tau_{\text{Th}}^i)]^2}, \quad (16)$$

we can finally achieve the best values for the (ν_0, r_0) pair. In the above equation, τ_{Exp}^i and τ_{Th}^i stand for the experimental and calculated alpha-decay half-life values, respectively, and w is the number of available experimental data. We have used 149 transuranic elements of the 443 experimental collected values from NUBASE2016 [40, 41] and references therein, obtaining the value of $\nu_0 = 1.1 \times 10^{22} \text{ s}^{-1}$ and $r_0 = 1.12 \text{ fm}$, providing a half-life rms standard deviation $\sigma = 0.56$. It is necessary to remark that all calculations performed in this work have been obtained under assumptions of ground-state to ground-state alpha transitions and no centrifugal barrier effects ($\ell = 0$).

The alpha half-life calculation is extremely sensitive to the Q_{α} -value, so that a significant uncertainty in Q_{α} -values may lead to large deviations in calculated half-life values. Therefore these half-life values can differ from data in a few orders of magnitude. In figure 4 we show

the results of the alpha-decay half-lives as a function of the atomic number and the number of neutrons of the parent nucleus. Figure 4(a) displays the calculated half-lives with Q_α -values extracted from the DZ model, while figure 4(b) presents results for Q_α^{BNN} -values. The remarkable difference between both panels is that a stability region around ^{284}Fl ($Z = 114$ and $N = 170$) appears in figure 4(a). This region is not reproduced in figure 4(b). The second difference lies in the location and topography of the region of the predicted nuclei of greatest stability. In figure 4(a) this region is located below $Z = 108$ and centered on $N = 184$, whereas in figure 4(b), this region changes and its center is located in a wider region, possibly between $106 \leq Z \leq 108$ and $N \geq 180$.

It is important to clarify that we are discussing the stability in respect to only one nuclear decay mode in the SHE region. For instance, the main decay mechanism of the Ds ($Z = 110$) seems to be the α -decay, although many different cluster emission modes can be competing with the α -decay process and contributing to total half-life [42–44]. For these modes, microscopic shell corrections of fragments are probably relevant. Thus a detailed study on other modes is welcome to better discuss the SHE stability near the $Z = 114$ and $N = 184$ region aforementioned.

7. Conclusions

In the present work, we constructed a correction function for the Q_α^{Th} -values by using the ten-parameter Duflo-Zuker mass model and a Bayesian neural network, and applied these values as input quantities for the calculation of alpha-decay half-life values in the context of the ELDM. This approach allowed us to improve the accuracy of the alpha released energy value as well as to provide theoretical predictions for alpha-decay half-lives closer to the experimental data. In addition, the implementation of the Bayesian neural network introduces new aspects correlated to the SHE magic numbers, which could not be observed in the theoretical description used, allowing the investigation of some possible internal structures of superheavy nuclei. A stating point to unveil the nuclear structure features enlightened by the BNN correction and associated with sub-magic or magic numbers is related to the following regions:

- $104 \leq Z \leq 106$: the neutron magic or sub-magic numbers are $N \sim 152, 162$ and 170 (see region (a) in figure 3).
- $107 \leq Z \leq 110$: $N \sim 162, 170$ and possibly 172 (see region (b) in figure 3).
- $111 \leq Z \leq 113$: $N \sim 170$ and possibly 172 (see region (c) in figure 3).
- $114 \leq Z \leq 117$: $N \sim 170$, possibly 172 and 184 (see region (d) in figure 3).
- $Z = 118$: possibly $N \sim 172$ and $N \sim 184$ (see region (d) in figure 3)
- $119 \geq Z$: the only possible magic or sub-magic number is $N \sim 184$.

All those candidates to magic numbers were previously reported (see [16] and references therein) except $N = 170$, which apparently is a product of the DZ model version used here. The present calculation has been performed for the entire superheavy nuclei region, and results showed that the region of greatest stability is located between $106 \leq Z \leq 108$ and $N \geq 180$.

Acknowledgments

The authors acknowledge the Coordenação de Aperfeiçoamento de Pessoal de Nível Superior (CAPES) for financial support. CZV thanks the Fundação de Amparo à Pesquisa e ao Desenvolvimento Científico e Tecnológico do Maranhão (FAPEMA) AUX-08355/17 for financial support. SBD thanks the Brazilian agency CNPQ for partial financial support.

Author contribution statement

All the authors were involved in the preparation of the manuscript and have contributed equally to the paper.

ORCID iDs

Sergio Barbosa Duarte  <https://orcid.org/0000-0003-0027-0230>

References

- [1] Oganessian Y T and Utyonkov V K 2015 *Rep. Prog. Phys.* **78** 036301
- [2] Oganessian Y T and Rykaczewski K P 2015 *Phys. Today* **68** 32
- [3] Karol P J, Barber R C, Sherrill B M, Vardaci E and Yamazaki T 2016 *Pure Appl. Chem.* **88** 155
- [4] Gamow G 1928 *Zeitschrift für Physik* **51** 204
- [5] Gurney R W and Condon E U 1929 *Phys. Rev.* **33** 127
- [6] Gonçalves M and Duarte S B 1993 *Phys. Rev. C* **48** 2409
- [7] Duarte S B and Gonçalves M G 1996 *Phys. Rev. C* **53** 2309
- [8] Gonçalves M, Duarte S, Garcia F and Rodríguez O 1997 *Comput. Phys. Commun.* **107** 246
- [9] Duarte S B, García F, Rodríguez O, Guzmán F, Tavares O A P and Gonçalves M 2002 *J. Phys. G: Nucl. Part. Phys.* **24** 1757
- [10] Gonçalves M, Rodríguez O, Guzmán F, Tavares O A P, Duarte S B and García F 2002 *J. Phys. G: Nucl. Part. Phys.* **26** 755
- [11] Duarte S B, Tavares O A, Guzmán F, Dimarco A, García F, Rodríguez O and Gonçalves M 2002 *At. Data Nucl. Data Tables* **80** 235
- [12] Duarte S B, Tavares O A, Gonçalves M, Rodríguez O, Guzmán F, Barbosa T N, García F and Dimarco A 2004 *J. Phys. G: Nucl. Part. Phys.* **30** 1487
- [13] Tavares O A, Medeiros E L and Terranova M L 2005 *J. Phys. G: Nucl. Part. Phys.* **31** 129
- [14] Medeiros E L, Rodrigues M M, Duarte S B and Tavares O A 2006 *J. Phys. G: Nucl. Part. Phys.* **32** B23
- [15] Duarte S B and Teruya N 2012 *Phys. Rev. C* **85** 1
- [16] Hofmann S and Münzenberg G 2000 *Rev. Mod. Phys.* **72** 733
- [17] Barber R C, Karol P J, Nakahara H, Vardaci E and Vogt E W 2011 *Pure Appl. Chem.* **83** 1485
- [18] Karol P J, Barber R C, Sherrill B M, Vardaci E and Yamazaki T 2016 *Pure Appl. Chem.* **88** 139
- [19] Wang M, Audi G, Kondev F G, Huang W, Naimi S and Xu X 2017 *Chin. Phys. C* **41** 030003
- [20] Gazula S, Clark J W and Bohr H 1992 *Nucl. Phys. A* **540** 1
- [21] Gernoth K A and Clark J W 1995 *Neural Netw.* **8** 291
- [22] Costiris N J, Mavrommatis E, Gernoth K A and Clark J W 2009 *Phys. Rev. C* **80** 044332
- [23] Bayram T, Akkoyun S and Kara S O 2014 *Ann. Nucl. Energy* **63** 172
- [24] Baldi P, Sadowski P and Whiteson D 2014 *Nat. Commun.* **5** 4308
- [25] Utama R, Piekarewicz J and Prosper H B 2016 *Phys. Rev. C* **93** 1
- [26] Bertsch G and Bingham D 2017 *Phys. Rev. Lett.* **119** 252501
- [27] Athanassopoulos S, Mavrommatis E, Gernoth K A and Clark J W 2004 *Nucl. Phys. A* **743** 222
- [28] Utama R, Chen W C and Piekarewicz J 2016 *J. Phys. G: Nucl. Part. Phys.* **43** 1
- [29] Utama R and Piekarewicz J 2017 *Phys. Rev. C* **96** 044308
- [30] Utama R and Piekarewicz J 2018 *Phys. Rev. C* **97** 1

- [31] Zhang H F, Wang L H, Yin J P, Chen P H and Zhang H F 2017 *J. Phys. G: Nucl. Part. Phys.* **44** 045110
- [32] Niu Z M and Liang H Z 2018 *Phys. Lett. B* **778** 48
- [33] Neufcourt L, Cao Y, Nazarewicz W and Viens F 2018 *Phys. Rev. C* **98** 1
- [34] Niu Z M, Liang H Z, Sun B H, Long W H and Niu Y F 2018 *Phys. Rev. C* **99** 064307
- [35] Neufcourt L, Cao Y, Nazarewicz W, Olsen E and Viens F 2019 *Phys. Rev. Lett.* **122** 062502
- [36] Neal R M 1996 *Bayesian Learning for Neural Networks, Lecture Notes in Statistics* vol 118 (New York, NY: Springer New York) p 204
- [37] Bishop C M 1995 *Neural Networks for Pattern Recognition* (Birmingham, UK: Oxford University Press)
- [38] Olsen E and Nazarewicz W 2019 *Phys. Rev. C* **99** 014317
- [39] Duflo J and Zuker A 1995 *Phys. Rev. C* **52** R23
- [40] Huang W J, Audi G, Wang M, Kondev F G, Naimi S and Xu X 2017 *Chin. Phys. C* **41** 030002
- [41] Cui J P, Zhang Y L, Zhang S and Wang Y Z 2018 *Phys. Rev. C* **97** 14316
- [42] Poenaru D N, Gherghescu R A and Greiner W 2012 *Phys. Rev. C* **85** 034615
- [43] Poenaru D N, Gherghescu R A and Greiner W 2011 *Phys. Rev. Lett.* **107** 995
- [44] Poenaru D N, Stöcker H and Gherghescu R A 2018 *Eur. Phys. J. A* **54** 14